



Potential of Inhibiting the Receptor Binding Mechanism of SARS-COV-2 using Phytochemicals contained in Paspanguwa Water Extract: Molecular Docking and Dynamic Studies

P.A.S.N.P. JAYAWARDENA^{1b}, A.M.S.C. SOORIYAWANSHA^{1b}, P.G.J.D. KUMARATHUNGA^{1b},
P.D.H. DANANJAYA^{1b}, C.C. KADIGAMUWA^{1b*} and J.N. DAHANAYAKE^{1b}

Department of Chemistry, University of Kelaniya, Kelaniya, Sri Lanka

*Corresponding authors: E-mail: cckadigamuwa@kln.ac.lk; jayangikadh@kln.ac.lk

Received: 5 May 2024;

Accepted: 28 October 2024;

Published online: 30 November 2024;

AJC-21828

This study is focused on the SARS-CoV-2 virus by *in silico* screening of phytochemicals contained in 'Paspanguwa' water extract, targeting ACE2 receptors using molecular docking. Phytochemicals of the five herbal ingredients contained in 'Paspanguwa' were extracted into water and were identified based on the literature reviews. Ligands geometries were optimized using Avogadro software and transformed to PDBQT format files by detecting torsion root using AutoDock Tools 1.5.6. SWISS-MODEL server was used to model the structure of the ACE2 receptor based on the UniProt ID Q9BYF1. The stereochemical quality of the protein model was assessed using SAVES v 6.0 and ProSA servers. Finally, potential ligands were docked to the ACE2 receptor protein by considering all variants of this virus and their interactions with the ACE2 receptor. The highest binding energy (BE) (-10.42 kcal/mol) was given by carpesterol phytochemical with allosteric site-2 and allosteric site-3 in the ACE2 receptor and this complex was subjected to molecular dynamic (MD) analysis using a CHARMM36 force field. According to the radius of gyration (Rg), root mean square deviation (RMSD) and root mean square fluctuation (RMSF) results, the studied protein-ligand complex was stable throughout the simulation time.

Keywords: ACE2 receptor, Molecular docking, Paspanguwa, Phytochemicals, SARS-CoV-2.

INTRODUCTION

Paspanguwa appears to be a traditional Sri Lankan home treatment that has been used for hundreds of years to treat common ailments such as common flu, influenza, fever, aches, pains, *etc.* and is mainly taken as herbal tea. The 'Paspanguwa' term comes from a combination of five primary herbs ('pas' = five, 'panguwa' = parts): ginger (*Zingiber officinale*), pathpadagam (*Hedyotis corymbosa*), katuwalbatu (*Solanum xanthocarpum*), venivalgata (*Coscinium fenestratum*) and coriander (*Coriandrum sativum*). Herbal ingredients contained in this mixture have to boil for nearly 15-20 min to extract all water soluble and heat-stable phytochemicals into water [1].

All of the herbs described above have their own unique characteristics. For example, the dry leaves and stems of Pathpadagam (*Hedyotis corymbosa*), contains active ingredients like phenolic acids, alkaloids, iridoids and flavonols [2]. Katuwalbatu (*Solanum xanthocarpum*) normally use whole plant parts to cure a variety of ailments [3,4], alkaloids, flavonoids, phen-

olics and tannin phytochemicals are the most important bioactive substances and also contains solasodine, which has antipyretic properties [1]. The decoction of dried berries contained in this herbal plant is used as an ingredient for the preparation of 'Paspanguwa'. Similarly, the dry stem of Venivalgata (*C. fenestratum*) contains berberine and shows hypoglycemic, antidiabetic, antibacterial, antioxidant and anticancer activities [1,5,6]. This herbal ingredient contains berberine. It belongs to the isoquinoline alkaloid type with a broad range of pharmacological properties.

COVID-19 is a disease produced by the SARS-CoV-2 virus and belong to RNA viruses with positive strands. It is classified as the *Coronaviridae* family. The nucleic material contains a bigger viral genome and its size range from 27 to 33 kbs. Several variations of SARS-CoV-2 are now circulating; some of them are proving to be deadly [7]. The clinical characteristics of this infection range from asymptomatic to acute respiratory distress syndrome and finally causing multi-organ failure. The main symptoms that occur due to this virus are shortness of

breath, trouble of breathing, fatigue, fever, headache, sore throat, nausea, diarrhea and loss of smell or taste. Pneumonia, respiratory failure, cardiac issues, liver problems and death can be caused by the SARS-CoV-2 virus. A condition known as cytokine storm or cytokine release syndrome may be the source of several COVID-19 problems [8].

For docking studies, the phytochemicals contained in the Paspanguwa' water extract were found based on the literature carried out. The ligands were docked to the SARS-CoV-2 virus spike protein binding site in the ACE2 receptor protein to predict whether there is a probability of chosen ligands interfering with the interaction between spike protein and ligand. For site specific docking, all types of variants and their interactions with ACE2 receptor protein were considered and the grid box was drawn to that site [9].

EXPERIMENTAL

Plant review: In accordance with the literature reviews, 60 ligands have been identified and the canonical SMILES of each ligand were then collected from the PubChem database (<https://pubchem.ncbi.nlm.nih.gov/>), respectively. Above Canonical SMILES were subjected to the SwissADME web server (<http://www.swissadme.ch/>) to check the drug-likeness properties. Ligands that followed Lipinski's rule of five were selected using this web server. Ligands did not have Canonical SMILES in the PubChem database and the structures were drawn in the SwissADME web server [10].

Ligands preparation: 3D structures of ligands were downloaded from the PubChem database in SDF format. Then the above files were subjected to Avogadro software and geometries were optimized using Force Field MMFF94, algorithm steepest descent, 500 steps. The files were then saved in PDB format and finally, PDB format files were subjected to AutoDock Tools 1.5.6 and converted into PDBQT file format [10].

Protein preparation: Based on the literature reviews, UniProt ID Q9BYF1 (<https://www.uniprot.org/>) was found for the human ACE2 receptor and the protein sequence of the ACE2 receptor was obtained from the UniProt website for the UniProt ID Q9BYF1. The protein sequence was run *via* the BLAST server (<https://blast.ncbi.nlm.nih.gov/>) and SWISS-Model online modeling server (<https://swissmodel.expasy.org/>) to find the homology sequences and thereby the template with higher GMQE, sequence similarity and higher sequence coverage was found. UniProt align server (<https://www.uniprot.org/align/>) was used to align the protein sequence with the modeled sequence and determined whether active sites and spike protein binding sites were conserved. Following the aforementioned information, the template was utilized in order to construct the protein model [10].

Model validation and refinement of model structure: After the modeled protein was built, the refinement was done by Galaxy Refine in the GalaxyWeb server (<https://galaxy.seoklab.org/cgi-bin/>). The protein was analyzed using ERRAT, Verify 3D, and PROCHECK from the SAVES v6.0 server (<https://saves.mbi.ucla.edu/>) and the ProSA server (<https://prosa.services.came.sbg.ac.at/>) was employed to validate the modeled structure [10].

Binding site identification: For site-specific docking, all types of SARS-CoV-2 virus variants and their interactions with ACE2 receptors were considered. The grid box was drawn to that site. The amino acids present in the binding pocket for the spike protein binding site in human ACE2 receptor are S19, Q24, T27, F28, D30, K31, H34, E35, A36, E37, D38, Y41, Q42, L45, L79, M82, P84, Y83, Q329, N330, K353, G354, D355, R357, R393 [11-13].

Molecular docking: Using AutoDock Tools 1.5.6, water molecules were eliminated, the polar hydrogen atoms were inserted and Kollman charges were added to the predicted protein structure. The file was then saved in PDBQT format. Then, ligand files were converted to PDBQT format files by identifying the torsion root. By sketching the grid at the binding site, ligands were docked into the protein's three-dimensional structure. Autogrid 4.2 created the map and grid parameter files. For docking studies, the Lamarckian genetic algorithm (LGA) was used. The following parameters were adjusted: the number of genetic algorithms (GA) runs: 100, the maximum number of energy evaluations: 5000000, the population size: 150 and the maximum number of 27,000 generations. AutoDock 4.2 (.dpf) is utilized for docking. The ligands were set to flexible and the protein adjusts as rigid. Finally, the resultant files were generated as (.dlg). After that the ligands that gave binding energy greater than -9 kcal/mol were docked to the same binding site to enhance the accuracy of these results [10].

Analysis of docking results: Interactions between protein-ligand complexes and amino acids located in the binding pocket were analyzed using the protein-ligand interaction profiler (<https://plip-tool.biotec.tu-dresden.de/plip-web/plip/index>), LigPlot and Pymol softwares.

Molecular dynamic (MD) simulation: MD simulations were performed using the GROMACS (version 2021.4) software package, with CHARMM36 force field and TIP3P water model. The protein-ligand complex was centered in a dodecahedron box with a minimum distance of 1.0 nm between the complex and any side of the box. The ligand topology was prepared using external tools of the CHARMM General Force Field server. The system was solvated with water and Na⁺ and Cl⁻ ions were added to replace solvent molecules, in order to neutralize the systems at 0.15 M salt concentration. The LINCS bond length constraint algorithm was used to constrain bond lengths. Particle Mesh Ewald summation was used for electrostatic interactions and grid spacing of 0.12 nm combined with an interpolation order of 4 was used for long-range interactions. For van der Waals interactions, a cut-off of 1.4 nm was used. Energy minimization was performed using the steepest descent algorithm. The system was gradually heated from 50 K to 300 K throughout a 100 ps time. Finally, the MD production run was done in NPT ensembles at 300 K using a V-rescale thermostat and at 1 bar using a Berendsen barostat. The results of the simulation were obtained after 10 ns production runs with 2 fs time steps. The trajectory obtained from the MD simulation was used to calculate the radius of gyration (Rg), root mean square deviation (RMSD) and root mean square fluctuation (RMSF).

RESULTS AND DISCUSSION

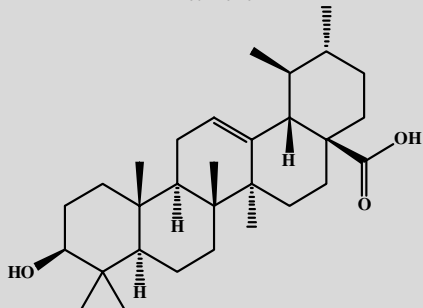
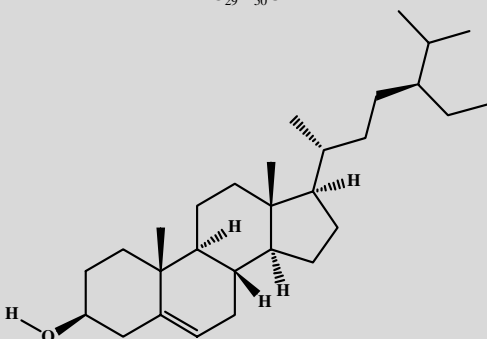
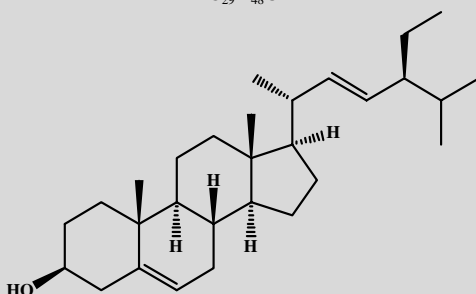
This study focused on the evaluation of antiviral activity against the SARS-CoV-2 virus by *in silico* screening of phytochemicals contained in 'Paspanguwa' water extract, by targeting ACE2 receptor using molecular docking and further, it was confirmed by molecular dynamics.

Ligands identification: Based on literature reviews, 61 phytochemicals were identified which were able to extract into water. Those phytochemicals were again filtered into 36 ligands based on their percentage amount extracted into water from each five ingredients and also with their drug-likeness properties. Phytochemicals that followed Lipinski's rule of five were chosen for the docking process. Lipinski's rule of five is used to determine whether drugs are orally active in humans. This rule further explains the molecular features of a drug that are important for its pharmacokinetics in the human body such as absorption, distribution, metabolism and excretion (ADME). Table-1 indicates that the phytochemicals exhibit superior

docking results (binding energy (kcal/mol) exceeding -9.00) and their drug-likeness characteristics derived from the Swiss-ADME online server. Several of these ligands violated one or two aspects of Lipinski's rule of five; yet, this web server approved them due to their minimal deviation from the established rule.

Model validation: Three-dimensional model of ACE2 was verified using the VERIFY 3-D score. By designating a structural class based on a structure's position and surroundings, it can be used to assess if an atomic model's (3D) correspondence with its corresponding (1D) amino acid sequence is valid. The outcomes are then contrasted with superior structures. The score of the passed residues, which was more than 0.2, served as a measure of the model's quality. The results show that the modeled protein has 94.64% of its average residues with a 3D-1D score greater than 0.2 (Fig. 1a). The statistics of inter-actions between different atom types that are not bound were evaluated using the ERRAT server. Scores of at least 60 are typically regarded as acceptable. The modeled protein had

TABLE-1
RESULTS OF PHYTOCHEMICALS HAVING HIGHER DOCKING SCORE
(BINDING ENERGY (kcal/mol) GREATER THAN -9.00) BASED ON LIPINSKI'S RULE OF FIVE

Compound	m.f. and structure	Lipinski's rule of five	
		Properties	Value
Urosilic acid	$C_{30}H_{48}O_3$ 	Molecular weight (g/mol) (< 500)	456.70
		H-bond donors (< 5)	2
		H-bond acceptors (< 10)	3
		Rotatable bonds (< 10)	1
		Log P_{ow} (< 5)	5.82
γ -Sitosterol	$C_{29}H_{50}O$ 	Molecular weight (g/mol) (< 500)	414.71
		H-bond donors (< 5)	1
		H-bond acceptors (< 10)	1
		Rotatable bonds (< 10)	6
		Log P_{ow} (< 5)	6.73
Stigmasterol	$C_{29}H_{48}O$ 	Molecular weight (g/mol) (< 500)	412.69
		H-bond donors (< 5)	1
		H-bond acceptors (< 10)	1
		Rotatable bonds (< 10)	5
		Log P_{ow} (< 5)	6.62

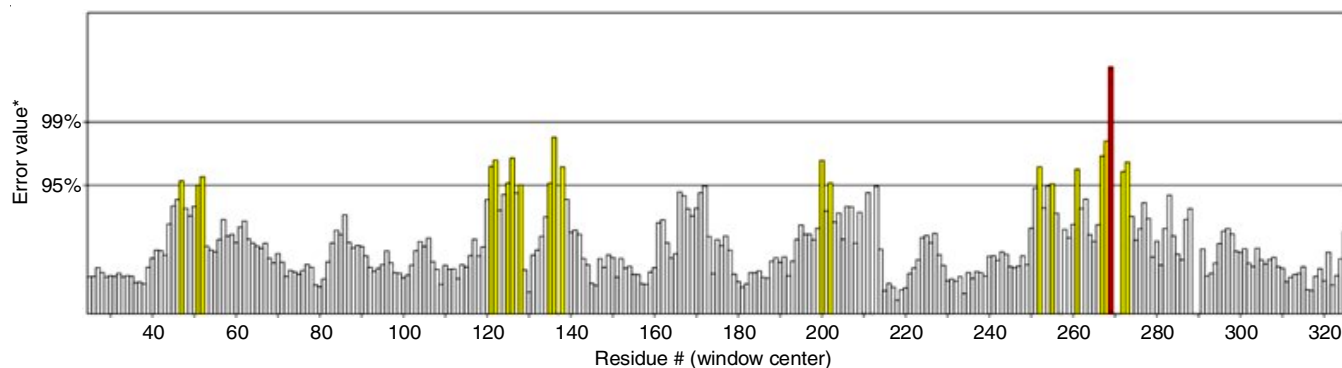
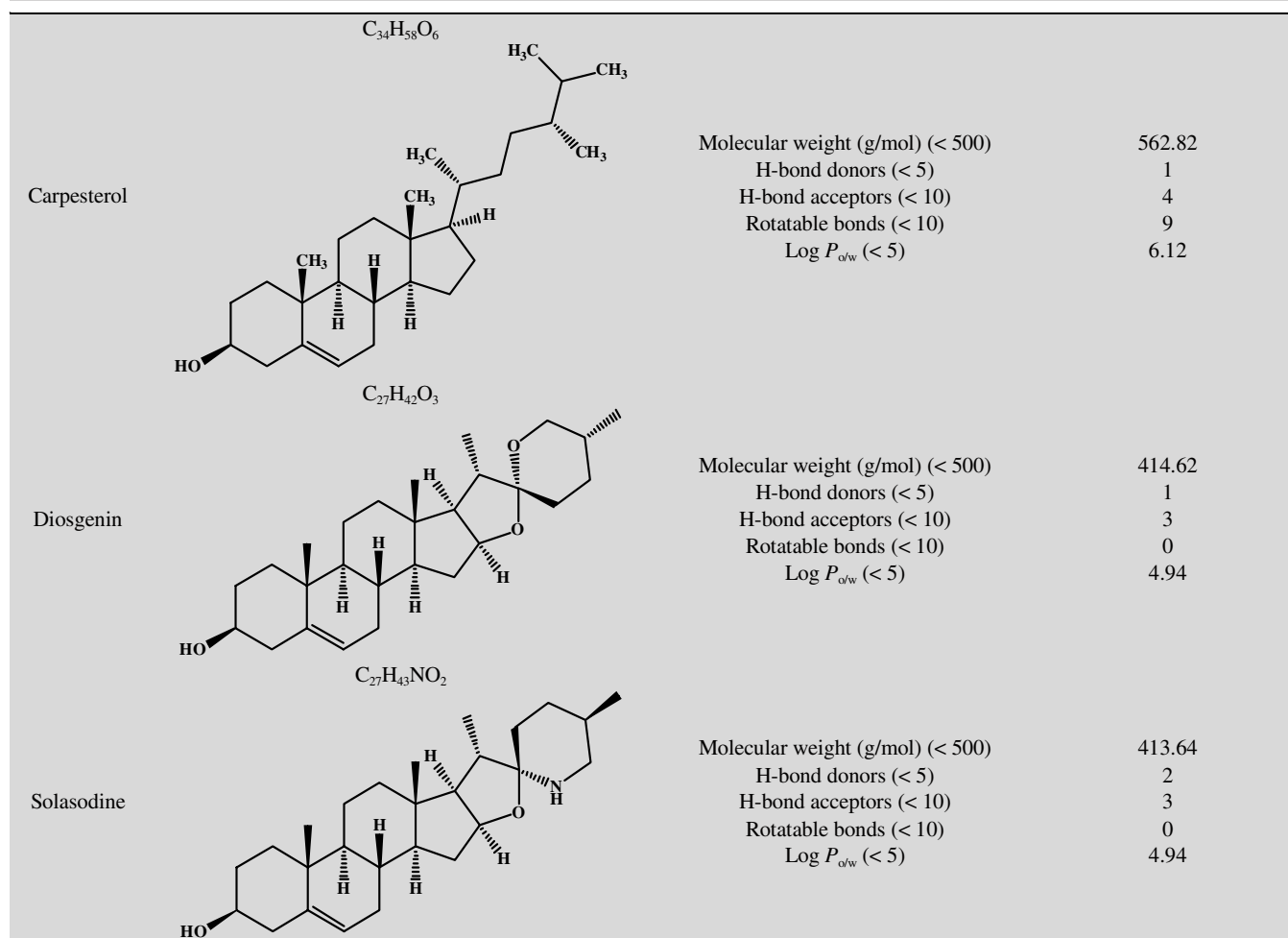


Fig. 1a. Precision of protein is shown by ERRAT plot (errors, cautions and acceptable scores are shown as red, yellow and white bars, respectively)

96.3% of its residues in the preferred region, which indicates that this structure is trustworthy for docking investigations (Fig. 1b). The modeled protein's ProSA score was -13.61, which confirmed its validity (Fig. 1c) [14].

Molecular docking studies: To determine the interactions between the proteins and the ligands, molecular docking can be done. The binding energies for each protein-ligand complex were retrieved using AutoDock 4.2 and the values are shown in Table-2. The docking results were obtained for site the specific rigid dockings by considering all types of SARS-CoV-2 virus variants spike proteins and their interactions with ACE2

receptor protein. Thirty-six ligands were docked to the site and out of that the binding energies of 20 ligands were greater than (-6.00 kcal/mol) (Table-3). The higher negative binding energies revealed that there were some stable protein-ligand complexes. However, it should be noted that binding energy alone cannot predict the effect on the target protein function. Each complex was evaluated using the protein-ligand interaction profiler and online web-based program to understand the relationships between complexes that showed the greatest binding energies. Amino acids involved in interactions with ligands are depicted in Table-3, only for those ligands that gave

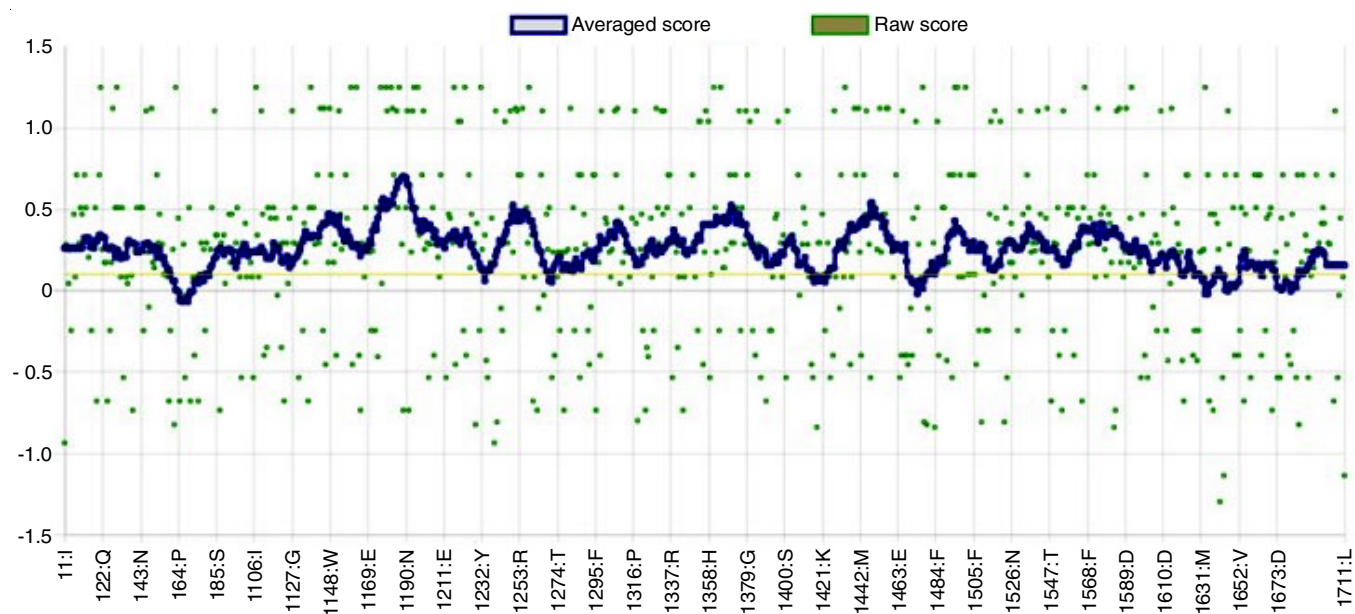


Fig. 1b. VERIFY3-D plot of ACE2-CARP complex

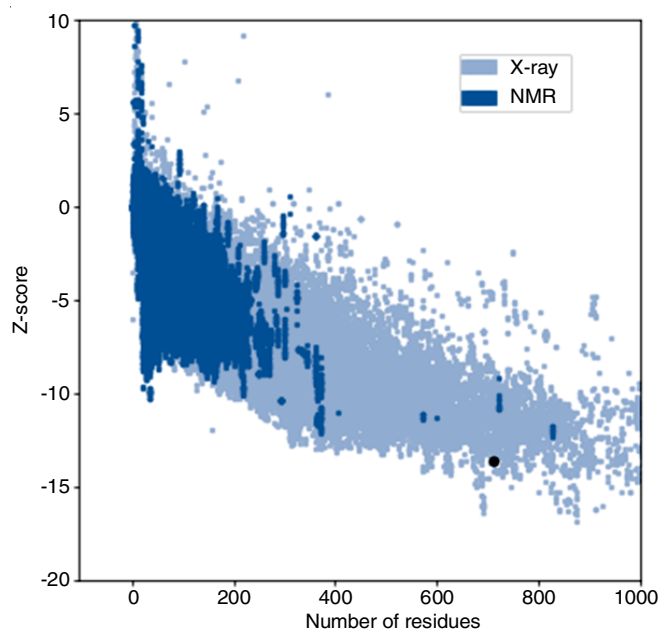


Fig. 1c. ProSA Z-score diagram of ACE2-CARP complex

binding energy greater than -7.00 kcal/mol. Pymol and LigPlot software were used to visualize the interactions and their results are depicted in Table-4 [15].

According to the interactions between ligands which were giving binding energies greater than -7.00 kcal/mol with virus spike protein binding site in ACE2 receptor, only ARG393 was implicated in interactions, as determined by interactions between ligands with the ACE2 receptor protein. The area, where the grid box was drawn, covered both allosteric site-2 and site-3. Phytochemicals that are attached to allosteric sites alter the structure of the protein. The biophysical interactions such as electrostatic and hydrogen bondings between the ACE-2 receptor and the viral receptor binding domain might be diminished by ligands that were docked to the allosteric areas

Compound	Ligand	Binding energy (kcal/mol)
Pathpadagam	Urosilic acid	-9.23
	6- α -Hydroxygeniposide	-5.59
	Asperulosidic acid	-5.36
	Biflorin	-6.35
	γ -Sitosterol	-10.11
	Geniposide	-6.63
Coriander	Oleanolic acid	-8.42
	Linalool	-5.69
	Limonene	-6.08
	Geranyl acetate	-5.37
	Geraniol	-5.58
	γ -Terpinene	-5.67
	Cineole	-6.52
	Camphor	-5.64
Ginger	α -Pinene	-6.39
	6-Gingerol	-5.04
	Zingiberene	-5.98
	β -Bisbolene	-5.97
	α -Curcumenne	-6.22
	6-Shogaol	-5.95
Venivalgata	6-Paradol	-5.87
	Berberine	-7.60
	Berberrubine Chloride	-6.62
	Jatrorrhizine	-6.54
	Palmatine	-6.61
	Sitosterol glucoside	-8.35
Katuwalbatu	Thalifendine	-6.57
	Berberrubine chloride	-6.62
	Stigmasterol	-10.19
	Apigenin	-6.75
	Carpesterol	-10.42
	Coumarin	-5.97
	Diosgenin	-9.18
Linoleic acid	-4.65	
Oleic acid	-4.10	
Solasodine	-10.34	

TABLE-3
LIGAND-PROTEIN INTERACTIONS INCLUDING THE TYPES OF INTERACTIONS THAT EACH AMINO ACID FAVOURS. NORMAL FONT REPRESENTS HYDROPHOBIC INTERACTIONS, *-REPRESENTS HYDROGEN BONDING AND – REPRESENTS SALT BRIDGES

Ingredient contains in paspanguwa	Ligand	Binding energy (kcal/mol)	Amino acids responsible for ligand-protein interactions
Katuwalbatu	Carpesterol	-10.42	PHE40A, TRP69A, LEU73A, LYS74A, GLU102A, PHE390A, LEU391A, ARG393A, SER77A*, ASN394A*, ARG393A
	Solasodine	-10.34	PHE40A, TRP69A, LEU73A, LEU100A, PHE390A, LEU391A, SER77A*, ARG393A*
	Stigmasterol	-10.19	PHE40A, LEU73A, ALA99A, LEU100A, TYR385A, PHE390A, LEU391A, ARG393A, SER77A*
	Diosgenin	-9.18	PHE40A, TRP69A, LEU73A, LEU100A, PHE390A, LEU391A, SER77A*
Pathpadgam	γ -Sitosterol	-10.11	PHE40A, LEU73A, ALA99A, LEU100A, TYR385A, PHE390A, LEU391A, ARG393A, SER77A*
	Urosilic acid	-9.23	LEU95A, GLN98A, GLN101A, GLN102A, GLU208A, GLN102A*, ASN103A*, ASN194A*, TYR196A*, GLU208A*, ASN210A*
	Oleanolic acid	-8.42	PHE40A, TRP69A, LEU73A, PHE390A, LEU391A, SER77A* PHE390A*, ARG393A*, ASN394A*
Venivalgata	Sitosterol glucoside	-8.35	PHE40A, TRP69A, TRP349A, ASP350A, PHE390A, LEU391A, ARG393A, SER77A*, LEU100A*, GLN102A*
	Berberine	-7.60	ASP206A, TYR207A, ASN397A, GLU398A, TRP566A, LYS562A*

of the receptor. Since the SARS-CoV-2 virus's binding amino acids (H345, H505, and R27313) are located in the protein's core, there is reasonable evidence that ACE-2 active site blockers were ineffective in preventing the virus's infection. Allosteric site 1 of ACE-2 is located directly below its active site. The interacting amino acid residues that often form hydrogen bonds with the SARS-CoV-2 receptor-binding domain are located close to the allosteric sites 2 and 3. Nearly all of the ligands bound to the specific amino acids found in allosteric site 2 and allosteric site 3, according to interactions between ligands that were giving binding energies more than -7.00 kcal/mol. Table-5 lists the amino acids that are present at allosteric sites 1, 2 and 3.

MD results: The protein-ligand complex with the lowest negative binding energy was subjected to MD simulations to investigate more about the ligand-protein interactions. According to Table-2, the lowest negative binding energy was represented by the spike protein binding site in the human ACE2 receptor (ACE2)-carpesterol (CARP) complex with -10.42 kcal/mol of binding energy. Following the completion of the MD simulation, a variety of output files were generated. Those were the trajectory file (all-atom positions in a series of snapshots or frames) and the energy file (values of kinetic and potential energy, pressure, temperature and other similar quantities over time). Those generated output files were used to analyze the system. In this study, qtgrace software was used for trajectory analysis. The root means square deviation (RMSD) and radius of gyration (Rg) of the protein ligand complex was determined to analyze conformational variations and stability. The flexibility of protein residues was obtained from root mean square fluctuation (RMSF).

Root mean square deviation (RMSD): The RMSD is defined as the spatial difference between two static structures of a trajectory file with the initial configuration of simulation. Here, the square root of the average deviation of all atoms of the complex over simulation time is considered. This calculation is used both as an indicator of the accuracy of the relevant protein-ligand complex and in order to ensure that the parti-

cular systems are in equilibrium and don't undergo any conformational changes. According to Fig. 2, the RMSD (nm) is shown *via* the Y-axis whereas stimulation time through picoseconds is given *via* the X-axis. Stimulation time for the complex is 10 ns. According to the RMSD plot, a flattering curve around ~0.75 nm explains the ACE2-CARP complex stability during the simulation period [16].

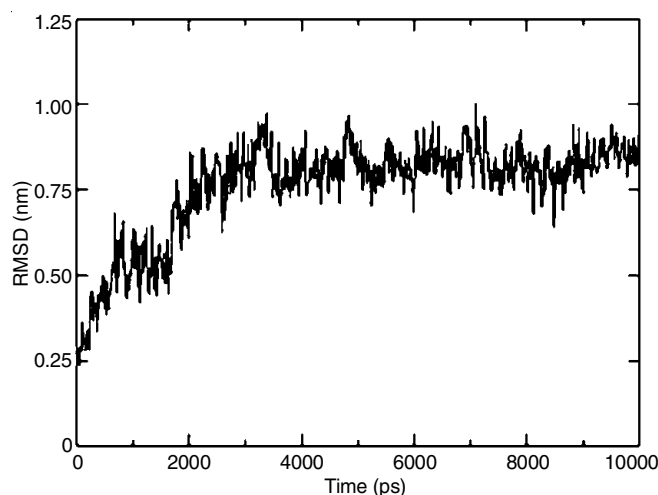


Fig. 2. Root mean square deviation (RMSD) plot of ACE2-CARP complex

Radius of gyration (Rg): Since the radius of gyration is a measure of protein compactness, it can be used to determine the stability or instability of the protein-ligand complex. After the MD simulation, the radius of gyration was analyzed to check whether the complex was stably folded or unfolded. It can be considered as a stable protein-ligand complex if the Rg value remains relatively constant throughout the MD simulation time; otherwise, it is considered unstable. According to Rg plot of the ACE2-CARP complex (Fig. 3), absence of the significant fluctuations and a steady curve around ~3.0 nm show ACE2-CARP complex stabilization during the simulation time of 10 ns [17].

TABLE-4
2D AND 3D IMAGES OF LIGAND-PROTEIN INTERACTIONS

Compound	2D visualization	3D visualization
Carpesterol*		
Solasodine*		
Stigmasterol*		

*Ligands that showed significant binding energy.

TABLE-5
LIST OF AMINO ACIDS PRESENT AT THE POTENTIAL ALLOSTERIC SITES OF ANGIOTENSIN-CONVERTING ENZYME 2

Allosteric sites	Surrounding amino acid residues
Allosteric site 1	PHE428, PRO289, ARG288, ASN290, GLU430, LEU418, PRO415, THR434, GLU435, ASN437, LYS541, THR414, MET366, PHE438, LEU439, LYS441, TYR279, ALA413, HIS540, CYSS542, ALA412, LEU539, ILE291, TYR587, GLN442, LEU410, LEU370, LEU526
Allosteric site 2	ALA396, ASN397, LEU392, SER563, GLU564, LYS562, TRP566, PRO565, LEU391, ASP206, VAL212, VAL209, GLU208, LEU91, GLN96, LEU95, ASN210, ALA99, GLN98, LYS94, LEU97, ILE88, LEU85
Allosteric site 3	PHE356, ASP355, ASP382, GLY354, ASP350, LEU351, TYR385, ALA386, GLY352, LYS353, ARG393, PHE390, PHE40, GLU37

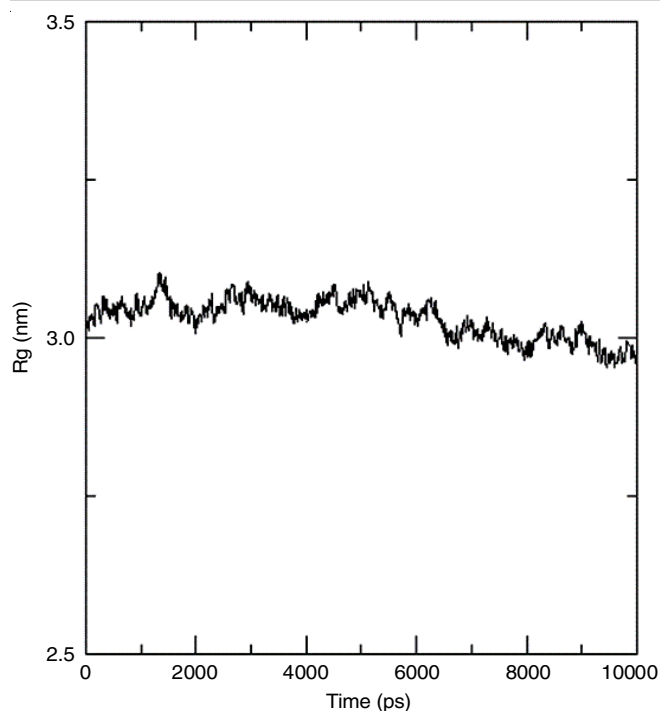


Fig. 3. Radius of gyration (Rg) plot of ACE2-CARP complex

Root mean square fluctuation (RMSF): According to the RMSF plot analysis of ACE2-CARP complex, significant fluctuation above ~ 0.40 nm residues explains that the disturbance for the interaction between ACE2 and CARP throughout the 10 ns of simulation time frame. But fluctuations between ~ 0.10 nm and ~ 0.20 nm residues belong to smooth interactions, due to the unchanging protein (ACE2) structure. The graph of RMSF per atom for the ACE2-CARP complex is shown in Fig. 4 [18]. According to the radius of gyration (Rg), root mean square deviation (RMSD) and root mean square fluctuation (RMSF) results, the studied protein-ligand complex was stable throughout the simulation time.

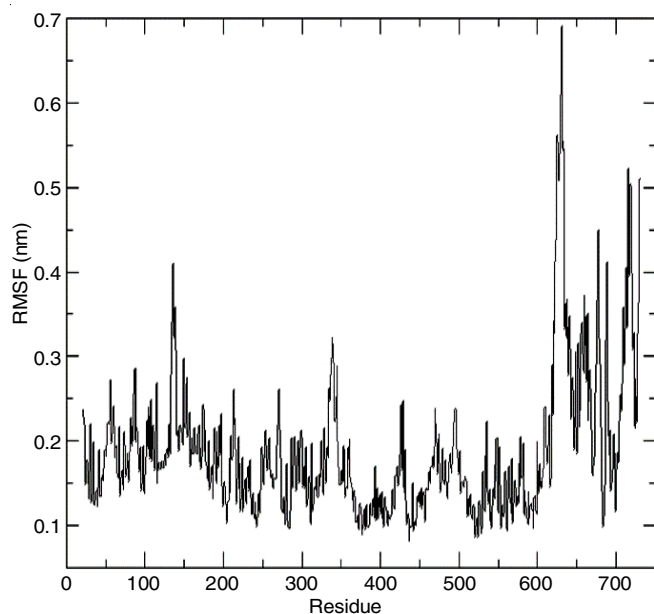


Fig. 4. Root mean square fluctuation (RMSF) plot of ACE2-CARP complex

Conclusion

Among the photochemicals presents in Paspanguwa water extract, stigmasterol, solasodine, carpesterol and γ -sitosterol showed greater affinities towards allosteric site 2 and allosteric site 3 in the ACE2 receptor with binding energies greater than -10.00 kcal/mol. These ligands might reduce biophysical interactions (such as electrostatic and hydrogen bonding) between ACE-2 and the viral receptor binding domain and disrupt hydrogen bonding formation between SARS-CoV-2 spike protein with ACE-2 receptor. Additional evidence for these findings was provided by molecular dynamic (MD) simulation of the protein-ligand complex ACE2-CARP, which had the highest binding energy. Therefore, the above results indicate there is a probability to cure COVID-19 by consuming Paspanguwa to a certain extent.

ACKNOWLEDGEMENTS

The authors thank Department of Chemistry, University of Kelaniya, Sri Lanka for providing research instruments for the experiments. Research fund provided by Faculty of Science, University of Kelaniya, under Research Grant no. RP/03/02/06/06/2021 is gratefully acknowledged.

CONFLICT OF INTEREST

The authors declare that there is no conflict of interests regarding the publication of this article.

REFERENCES

- H.K.S. De Zoysa, P.N. Herath, R. Cooper and V.Y. Waisundara, *J. Complement. Med. Altern. Health.*, **3**, 2 (2017); <https://doi.org/10.19080/JCMAH.2017.03.555609>
- H. Otsuka, K. Yoshimura, K. Yamasaki and M.C. Cantoria, *Chem. Pharm. Bull.*, **39**, 2049 (1991); <https://doi.org/10.1248/cpb.39.2049>
- S. Joghee, *Int. J. Pharmacogn. Chinese Med.*, **3**, 1 (2019); <https://doi.org/10.23880/ijpc-16000177>
- M. Nithya, C. Ragavendran and D. Natarajan, *Int. J. Food Prop.*, **21**, 313 (2018); <https://doi.org/10.1080/10942912.2017.1409236>
- V. Danapur, C. Haleshi and A.N. Sringswara, *Pharmacogn. J.*, **12**, 1077 (2020); <https://doi.org/10.5530/pj.2020.12.152>
- S.W. Goveas and A. Abraham, *Asian J. Pharm. Clin. Res.*, **6**, 218 (2013).
- G. Sgorlon, T.P. Roca, A.M.P. Silva, M.G.F. Custodio, J.A.D.S. Queroz, A.L.F.D. Silva, K.S. Teixeira, F.S. Batista, J.M.V. Salcedo, R.D.C.P. Rampazzo, F.G. Naveca and D. Vieira, *Bioinform. Biol. Insights*, **17** (2023); <https://doi.org/10.1177/11779322231186477>
- M. Ogolodom, A.N. Mbaba, N. Alazigha, E.O. Felix, N.O. Egbe, I. Golden, C.M. Eke and A.G. Ikechi, *Health Sci. J.*, **Sp.Iss.1**, 002 (2020); <https://doi.org/10.36648/1791-809X.S1.002>
- X. He, W. Hong, X. Pan, G. Lu and X. Wei, *MedComm*, **2**, 838 (2021); <https://doi.org/10.1002/mco2.110>
- N. Hansini, A.M.S.C. Sooriyawansa, P.A.S.N.P. Jayawardena, P.G.J.D. Kumarathunga, P.D.H. Dananjaya, E.A.C.P. Edirisinghe, M.N.D. Alwis, D.A. Daranagama, J.N. Dahanayake and C.C. Kadigamuwa, *Med. Plants - Int. J. Phytomedicines Relat. Ind.*, **15**, 677 (2023); <https://doi.org/10.5958/0975-6892.2023.00068.0>
- B. Jawad, P. Adhikari, R. Podgornik and W.Y. Ching, *J. Chem. Inf. Model.*, **61**, 4425 (2021); <https://doi.org/10.1021/acs.jcim.1c00560>

12. T. Jordá and S. Puig, *Genes*, **11**, 795 (2020); <https://doi.org/10.3390/genes11070795>
13. J. Low-Gan, R. Huang, A. Kelley, G.W. Jenkins, D. McGregor and V.V. Smider, *Biochem. J.*, **478**, 3671 (2021); <https://doi.org/10.1042/BCJ20200908>
14. J. Pra•nikar, M. Tomiæ and D. Turk, *Sci. Rep.*, **9**, 1678 (2019); <https://doi.org/10.1038/s41598-019-38658-9>
15. F.N. Novikov and G.G. Chilov, *Mendeleev Commun.*, **19**, 237 (2009); <https://doi.org/10.1016/j.mencom.2009.09.001>
16. K. Sargsyan, C. Grauffel and C. Lim, *J. Chem. Theory Comput.*, **13**, 1518 (2017); <https://doi.org/10.1021/acs.jctc.7b00028>
17. P. Sneha and C.G. Priya Doss, *Adv. Protein Chem. Struct. Biol.*, **102**, 181 (2016); <https://doi.org/10.1016/bs.apcsb.2015.09.004>
18. H.L. Barazorda-Ccahuana, D.E. Valencia, J.A. Aguilar-Pineda and B. Gómez, *ACS Omega*, **3**, 17254 (2018); <https://doi.org/10.1021/acsomega.8b02288>